Journal of the European Ceramic Society 42 (2022) 4631–4642

Contents lists available at ScienceDirect

Journal of the European Ceramic Society

journal homepage: www.elsevier.com/locate/jeurceramsoc

Microstructure, residual stresses, and mechanical performance of surface crystallized translucent glass-ceramics

Débora Cristina Niero Fabris [a,b,c,*], Enzo Henrique Miguel [b], Rafael Vargas [a,d], Rodrigo Bresciani Canto [a], Mariana de Oliveira Carlos Villas-Boas [a,b], Oscar Peitl [b], Vincenzo M. Sglavo [c], Edgar Dutra Zanotto [a]

[a] Graduate Program in Materials Science and Engineering (PPGCEM), Department of Materials Engineering (DEMa), Federal University of São Carlos (UFSCar), São Carlos, SP 13.565-905, Brazil

[b] Center of Research, Technology, and Education in Vitreous Materials (CeRTEV), Department of Materials Engineering (DEMa), Federal University of São Carlos (UFSCar), 13565-905, São Carlos, SP, Brazil

[c] Department of Industrial Engineering, University of Trento, Via Sommarive 9, Trento, Italy

[d] Université Paris-Saclay, ENS Paris-Saclay, CNRS, LMT - Laboratoire de Mécanique et Technologie, 91190 Gif-sur-Yvette, France

ARTICLE INFO

Keywords:
Crystallization
Glass-ceramic
Surface
Residual stress
Mechanical property

ABSTRACT

Mechanical properties of glasses can be significantly increased by inducing surface crystallization of a low coefficient of thermal expansion phase. In this work, we produced surface crystallized lithia-alumina-silica glass-ceramics with different crystallized layer thicknesses and analysed the resulting residual stresses and their effect on mechanical properties. The residual stress magnitude was estimated by *analytical* and *experimental* methods, as well as *numerical* modeling. The surface compressive stress reached 390 MPa and 490 MPa, as given by the analytical and experimental determination, respectively. These stresses prevented radial cracking in microhardness and scratch tests. The best glass-ceramic achieved a Vickers hardness of 7.5 GPa and fracture strength of 680 ± 50 MPa in a ball-on-three-ball test. These glass-ceramics are *translucent*, providing 50–60% transmittance over the visible wavelength spectrum (1.3 mm-thick-sample). This study unveiled the causes of improved mechanical properties and validates the concept that surface crystallization is a valuable technique for developing high strength glass-ceramics.

1. Introduction

An updated definition of glass-ceramics (GCs) reads: *Glass-ceramics are inorganic, non-metallic materials obtained by controlled crystallization of glasses, which can result in properly designed nano or microstructures with one or more crystal phases dispersed in the sample interior or on the* ***surface****. These materials have one or more functional crystalline phases and residual glass with crystallized fraction spanning from a few ppm to almost 100%* [1]. Certain high-performance glass-ceramics are useful for applications that require transparency and may undergo severe mechanical solicitation, such as safety transparent materials, *e.g.*, for ballistic protection or electronic device screens. Most GCs present significantly better mechanical performance than their parent glasses [2,3].

This research explores one crystallization route that might lead to the development of very strong, translucent GCs to be used, *e.g.*, as device screens. The main complaint of smartphone users is screen breakage, representing 22% of all answers [4]. Another common problem refers to scratches. Hence, in this context, such materials should combine high impact and scratch resistance [4–8]. The fracture resistance of current display glasses is generally obtained through an ion exchange process, which induces a compressive layer on the material surface due to substituting small ions of the glass for larger ones, *e.g.*, Na^+ or Li^+ by K^+ contained in a molten salt [4,7,9]. However, this method is limited to relatively soft glasses due to the nature of the alkali ions that are able to undergo the ionic exchange (IOEX) process and that should be present in large amounts in the glass composition. Smartphone screens, such as the Gorilla glass Victus, although characterized by very high flexural strength, have a Vickers hardness of approximately 6 GPa or less, a relatively low value that limits its scratch resistance [10]. Moreover, for this particular application, the material should be resistant to bending

* Corresponding author at: Graduate Program in Materials Science and Engineering (PPGCEM), Department of Materials Engineering (DEMa), Federal University of São Carlos (UFSCar), São Carlos, SP 13.565-905, Brazil.

E-mail address: deboracnfabris@gmail.com (D.C.N. Fabris).

https://doi.org/10.1016/j.jeurceramsoc.2022.04.024
Received 23 November 2021; Received in revised form 30 March 2022; Accepted 11 April 2022
Available online 14 April 2022
0955-2219/© 2022 Elsevier Ltd. All rights reserved.

fracture and impact, which are related to toughness (K_{IC}) and fracture strength [6,11,12]. Recently, a novel glass-ceramic (Ceramic Shield) was launched for the iPhone 12 screen display, which is stronger than any type of IOEX glass [13] used in smartphone displays. Mohs hardness tests indicate it scratches at level 6 [14], which corresponds to the orthoclase mineral (6.9 ± 0.7 GPa Vickers hardness) [15], somewhat higher than that of soda-lime-silica glass of 5.4 GPa [16].

Surface crystallization is an alternative method to enhance the mechanical properties of certain glasses. The phases crystallized in such GCs (generally) account for better mechanical properties than the parent glasses. Moreover, when the crystalline surface layer has a lower coefficient of thermal expansion (CTE) than the core glass, *compressive* stresses are generated on the surface after cooling down from the thermal treatment temperature [17,18]. These compressive stresses further improve the material's strength (S_f), hardness and damage resistance.

It is surprising that very few studies have been performed on this particular strengthening mechanism. To the best of our knowledge, the most promising surface crystallized GC launched so far seems to be the Lithium Aluminum Silicate (LAS) glass-ceramic proposed in the 1990 s by Priller, Frischat and Pye [17], a GC containing β-spodumene or β-eucryptite on the surface. The average CTEs of such crystal phases are approximately one order of magnitude lower than that of the base glass, which resulted in an impressive improvement of the bending strength, of 400%, reaching 800 MPa. The authors also suggested that a ~90 μm thick crystallized layer is most beneficial to increase the flexural strength. A large number of patents demonstrating improved strength by surface crystallization can also be found, *e.g.* [19–22]. They are mostly based on the LAS system with β-spodumene or quartz-ss crystallization. The first patent was granted in the 60 s [20], and proposed a method for surface compression through random surface crystallization. Nonetheless, application of these materials is still challenging.

Crystals with low average CTEs are obtained when the thermal expansion coefficient is negative along one specific crystallographic axis. However, such high CTE anisotropy also might lead to spontaneous crack development in the material [23,24]. According to Pelletant et al. [23], the β-eucryptite grain size influences the cracking behavior. For instance, the critical grain size for self-cracking is approximately 2.8 μm in pure β-eucryptite ceramics obtained by conventional pressing and sintering [23]. The crystal lattice CTEs of this phase from room temperature to 800 °C are: $\alpha_a = 8.1 \times 10^{-6}\,°C^{-1}$ and $\alpha_c = -17.6 \times 10^{-6}\,°C^{-1}$, and the average, macroscopic linear CTE of the glass-ceramics are $0.6 \times 10^{-6}\,°C^{-1}$, $-0.5 \times 10^{-6}\,°C^{-1}$ and $-0.3 \times 10^{-6}\,°C^{-1}$ for average grain sizes of 2.8 ± 0.6, 7.3 ± 0.4 and 13.2 ± 1.0 μm, respectively [23].

Similarly, Shyam, Muth and Lara-Curzio [24] observed that a bulk crystallized β-eucryptite glass-ceramic with a grain size below 4 μm did not crack. On the other hand, samples with grain sizes of 8 and 23 μm spontaneously cracked.

Surface crystallization negative CTE phases on glasses of the system $BaO\text{-}SrO\text{-}ZnO\text{-}SiO_2$ was evaluated by Waurischk, Thieme and Russel [25]. They reported that an increase in the crystallization temperature leads to a randomly distributed crystal orientation, whereas low temperatures favour crystal texture.

Kracker et al. [26] studied surface crystallization of $Ba_{0.5}Sr_{0.5}Zn_2Si_2O_7$ on a $8BaO.8SrO.34ZnO.50SiO_2$ glass and observed a strong texture; the c-axis of the 10–100 μm crystals grew perpendicularly to the sample surface. In this case, the c-axis CTE is highly positive ($30 \times 10^{-6}\,°C^{-1}$), whereas the b-axis is negative ($-20 \times 10^{-6}\,°C^{-1}$), resulting in cracks parallel to the specimen surface. In these four references there is no information about the residual stress level achieved and the fracture strength of the resulting glass-ceramics.

1.1. Objectives

LAS glass-ceramics can reach Vickers hardness up to 8.5 GPa [27], making them a possible (harder) substitute for the electronic device screens, if one could produce transparent or, at least, highly translucent GCs in this way. To the best of our knowledge, there is no published report concerning the application of *translucent* surface crystallized glass-ceramics for electronic device screens. To evaluate such a possibility, a study of the relationship between thermal treatment, microstructure, residual stresses and mechanical behavior of this particular type of glass-ceramic is highly desirable. Furthermore, the Finite Element Method can be straightforwardly used to predict the residual stress fields developed due to crystallization, and their effect on the overall mechanical behavior [28,29]. Therefore, this work aims to fill this gap by evaluating the possibility of developing a crystallization strategy for a translucent, hard and strong surface crystallized glass-ceramic. Here we significantly expand and test the hypothesis shaped by Priller, Frischat and Pye [17] by using analytical, numerical, and experimental methods. In particular, we focus on understanding the relationships between thermal treatment, microstructure, residual stress level and mechanical performance.

In the next section, we describe the materials and methods used. Then, we show the governing equations and the FEM approach for evaluating the stress fields. In the Results section, we analyse the glass crystallization process; the resulting microstructures, the influence of the low CTE surface layer thickness on the generated compressive stresses and on the overall mechanical behavior of the glass-ceramics. Lastly, we discuss a recurrent problem with these surface crystallized GCs, *i.e.,* why and how a crystalline layer sometimes leads to spontaneous shattering. Finally, we summarize the most important findings and suggestions for future works.

2. Materials and methods

The glass composition used here was proposed in Ref. [17]: $66.0SiO_2\text{-}20.7Al_2O_3\text{-}6.1Li_2O\text{-}2.9\ K_2O\text{-}2.0Na_2O\text{-}1.2MgO\text{-}1.1CaO$ (wt%). This composition was selected due to the possibility of achieving very high flexural strength (up to 800 MPa) for the resulting GCs. In this work, we significantly extended the thermal treatment protocol and attempted to understand the effect on the resulting microstructure, compressive residual stresses and mechanical properties.

The chemicals SiO_2 (Vitrovita, <99.98%), Al_2O_3 (Almatis, 99%), Li_2CO_3 (Alfa Aesar, 99%), K_2CO_3 (Alfa Aesar, 99%), Na_2CO_3 (Alfa Aesar, 98%), MgO (Sigma Aldrich, 98%) and $CaCO_3$ (Alfa Aesar, 98%) were weighted, wet mixed in a ball-mill during 3 h, dried, and melted at 1630 °C during 4 h in a platinum crucible. The melted glass was splat-cooled, ground and remelted three times for homogenization. The liquid was cast into a 14 × 50 mm cylindrical steel mold to prepare specimens for Ball-on-Three-Balls (B3B) tests [30], generating 8 cylindrical pieces. The glass cylinders were annealed during 4 h at 530 °C (T_g ~560 °C) to remove residual stresses.

The thermal behavior of the glass was evaluated by Differential Scanning Calorimetry (DSC) at 10 °C/min using ~20 mg of a powder and a bulk sample (NETZSH DSC 404). The glass transition temperature (T_g) and crystallization peak (T_c) were used to define the thermal treatments.

The glass stability parameter (K_m) of this glass [$K_m = (T_x\text{-}T_g)^2/T_g$] is ~7. This value is much lower than that of several dental glass-ceramics being studied in our laboratory, LaMaV [31,32]. According to Jiusti et al. [31,33], for $K_m < 10$ the glass-forming ability (GFA) is low. Hence, this glass can only be made in relatively thin samples, which would be adequate for thin electronic displays.

A 2^2 central point factorial design was used to optimize the thermal treatment (time and temperature) required to obtain a fully crystallized surface. The layer depth, surface crystallized fraction, and grain size were measured by optical microscopy (Leica DMRX). The crystallized layer was observed in the transversal direction of glass-ceramic pieces, which were polished and etched with a 2 vol% HF solution for 10 s to reveal the crystals. The measurements were made using the ImageJ software for obtaining the linear thickness perpendicular to the sample surface. At least 100 measurements were taken at each condition to

obtain the average thickness and dispersion.

The crystal phases on the specimen surface were identified through X-ray diffraction (XRD) using a Rigaku model Ultima IV equipment. The scanning conditions were the step of 0.02° and a speed of 0.5°/min from 10° to 60°, using Cu-Kα radiation. The phases were identified using the Inorganic Crystal Structure Database (ICSD).

The optical absorbance from the ultraviolet to the near-infrared of the parent glass and GC (590 °C/6 h) were measured using a Perkin Elmer, model Lambda 25 spectrophotometer. One 1.3 mm thick polished sample for each condition was measured three times from 190 to 1100 nm. The sample was placed between the light source and the reader, at 34 and 86 mm, respectively.

The cylindrical parent glass pieces were cut in discs of 14 mm in diameter and 1.3 mm in thickness, grinded and polished with a 3 μm-cerium oxide suspension for the ball-on-three balls (B3B) tests. Five samples were tested for each crystallized layer thickness. The tests were conducted using 8 mm steel balls, with a loading rate of 1 mm/min (MTS criterion Model C 43.104). The equivalent stress before breaking, considering a homogeneous elastic material, was calculated according to:

$$\sigma_{eq} = f(\alpha, \beta,)\frac{F}{e^2} \tag{1}$$

$$f\left(\frac{e}{R}, \frac{R_a}{R},\right) = c_o + \frac{\left(c_1 + c_2\frac{e}{R} + c_3\left(\frac{e}{R}\right)^2 + c_4\left(\frac{e}{R}\right)^3\right)}{1 + c_5\frac{e}{R}}\left(1 + c_6\frac{R_a}{R}\right) \tag{2}$$

where e is the thickness, F is the rupture load, R sample radius, Ra is sphere radius, ν is the Poisson ratio and c0, c1, c2, c2, c3, c4 e c5 are coefficients depending on ν. β (Ra/R) and the α (e/R) factors should be between 0.55 and 0.9 and 0.05–0.6, respectively.

The Young's modulus, E, of the parent glass was determined by the sound propagation method (Sonelastic, ATCP Engenharia Física, São Carlos) using circular plates of 12 × 1.2 mm^2. The Young's modulus of the residual glass was estimated using the Sci-glass software. Its composition was calculated considering that all Al_2O_3 of the parent glass was consumed during the crystallization of β-spodumene, thus resulting in the following composition: 71.3SiO_2-0.2Al_2O_3-0.5Li_2O-7.6K_2O-8.0Na_2O-7.6MgO-4.8CaO (mol%). The value calculated by the Priven-2000 method is 67 GPa.

Nanoindentation tests were carried out to evaluate the mechanical properties of the crystallized layer using Anton Paar NHT equipment with a Vickers diamond tip. The samples were tested with a loading and unloading rate of 0.16 N/min, and a dwell time of 10 s at the maximum load of 0.08 N. At least eight valid indentations were made in each glass-ceramic and five indentations in the parent glass. The nanohardness (H_{IT}) was determined by the Oliver & Pharr method [34]. The elastic modulus on plane stress (E *) and indentation elastic modulus (E_{IT}) were calculated as:

$$E_r = \frac{\sqrt{\pi}\bullet S}{2\delta\bullet\sqrt{A_p(h_c)}} \tag{3}$$

$$E* = \frac{1}{\frac{1}{E_r} - \frac{1-\nu_i^2}{E_i}} \tag{4}$$

$$E_{IT} = E\bullet\left(1 - \nu^2\right) \tag{5}$$

where E_r is the reduced elastic modulus, E_i and ν_i are the elastic modulus and Poisson ratio of the indenter, respectively, β is a factor that depends on the indenter geometry ($\delta = 1.012$ for pyramidal square base), S is the contact stiffness, evaluated from the slope of the unloading curve, A_p is the contact area and hc is the maximum indenter penetration depth.

Vickers indentation experiments were carried out on the LAS parent glass, glass-ceramics and a commercial window glass using a Future Tech FM-700 hardness tester using loads from 0.98 N to 19.6 N. Micrographs of indentations were taken 1 h after the test. At least five indentations were made in each condition up to 4.9 N. Above this load, the imprints were quite cracked, but the measurements were taken for comparison purposes.

Scratch tests were carried out using an Anton Paar NHT equipment with a 100 μm radius Rockwell indenter (diamond cone of 120° with a 100 μm tip radius). An increasing load was applied from 0.3 to 20 N in 2 mm distance, with stress rate of 9.98 N/min.

The toughness of the parent glass was preliminarily estimated by the indentation method (K_C), which is known as indentation crack resistance. The radial cracks generated by 19.6 N indentations were measured and the K_C was estimated by the following equation [35]:

$$K_c = 0.016\sqrt{\frac{E}{H}}\left(\frac{P}{c^{3/2}}\right) \tag{6}$$

where H *is* the hardness, P is the indentation load, and c is the radial crack length. The ratio c/a was ≥ 2.5 in all measurements (***a*** is the half diagonal of the hardness imprint).

Governing equations and surface stress calculation.

The residual stresses developed after cooling were studied by analytical and numerical methods. These values were compared to the fracture stress increments determined by B3B.

The surface stress generated by the crystallization was calculated as: [17].

$$\sigma_s = \frac{E}{(1-\nu)}\left(T_g - T_{amb}\right)\left(\alpha_s - \alpha_i\right)\frac{A_i}{A_t} \tag{7}$$

where T_{amb} is the room temperature, α_s is the average thermal expansion coefficient of the crystallized layer (surface), α_i is the thermal expansion coefficient of the residual glass (interior), A_i is the internal cross section area, and A_t is the total cross section area.

The numerical model was evaluated using the Finite Element Method (FEM) with the commercial software Abaqus®. The mechanical parameters are presented in Table 1. The first model consists of an axisymmetric simulation with boundary conditions, as shown in Fig. 1, and simulates the stress generated during cooling from T_g to room temperature. The region adopted for the simulations was one-quarter of the transversal section of a 1.3 × 14 mm disc, as shown in Fig. 1a, using an axisymmetric model. The crystalline layer thickness was varied from 5 to 350 μm, using a 2D representation of the glass surface divided into around 175,000 four node axisymmetric elements (CAX4).

For the purposes of these approximate simulations, the E and α were defined as isotropic. The E and ν values for the residual glass (E_{gres} and ν_v) and crystal (E_c and ν_c) were assumed to be equal as their difference is small. A convergence analysis was performed for every simulated case to

Table 1
Parameters used to calculate the residual stresses by the analytical and numerical methods.

Property	Value
α_i (°C^{-1})	7.35 E-06
α_s (°C^{-1})	-5.00 E-07
T_i (°C)	565
T_f (°C)	30
ν_c, ν_g (adimensional)	0.23
E_g, E_c (GPa)	77
E_{gres} (GPa)	67

Where: α_i = Residual glass linear thermal expansion coefficient; α_s = Surface layer linear thermal expansion coefficient; T_i = Temperature in the sample interior; T_f = Temperature of the surface crystallized layer; ν_c = Crystal phase Poisson ratio; ν_g = glass Poisson ratio; E_g = Young's modulus of the glass; E_c = Young's modulus of the crystallized phase; E_{gres} = Young's modulus of the residual glass.

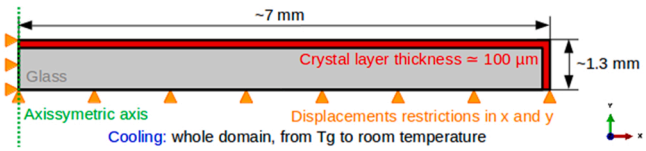

Fig. 1. Geometry and boundary conditions for the FEM axisymmetric model.

ensure no dependence on the element size.

To further study this phenomenon, we tested two types of simulations. First, an axisymmetric model was used to test for border effects of a constant crystal layer in one disk. The geometry and boundary conditions are presented in Fig. 1, with the axisymmetric axis (the revolution axis for the geometry) in the left, and a symmetry condition at the bottom, *i.e.,* one quarter of the sample cross section was drawn. This first simulation consists of a simple cooling from the T_g (565 °C) to room temperature (30 °C) to analyse the residual stresses. This first model led to some insights about the rounding of the sample corners and also about the crystalline layer in the disk lateral to simplify the following 3D analysis.

Then, the 3D model shown in Fig. 2 is used. This model had both crystalline layers at the disk top and bottom, but not in the lateral (due to its very small influence). A similar cooling step was first applied to estimate the residual stresses in the layers. In the second step, the loading was prescribed as a displacement in the disk center at the top (in the negative y direction, see Fig. 2a) with three static supports at the bottom (with displacements blocked in the y direction, see Fig. 2b), to simulate the B3B experiment. Rigid body motion was blocked for x and z directions. The model consists of ~260,000 C3D8R elements (Fig. 2c). We also show in Fig. 2d the outer crystal layers that consist of four elements in the thickness and the elements in the disk center, where the stresses were analysed, approximately 20 µm cubes. Although ref. [30] provides analytical equations for the B3B, the assumption of a homogeneous material is not valid herein (apart from the original glass sample without the crystal layer). Thus, the glass strength was obtained from the maximum principal stress in the simulation of the glass sample (without crystal layers) in the step where the reaction force reaches the experimental ultimate force. For the other cases with the outer crystal layers, the reaction force was taken for the step that the outer layer has the maximum stress level equal to the glass strength, and, thereby, could not further support the internal stresses.

3. Results and discussion

3.1. Crystallization behaviour

The thermal behavior of the parent glass as obtained by DSC analysis and the crystallized phase observed by DRX are shown in Fig. 3.

The parent glass powder shows the T_g (onset) at 560 °C and the T_c at 655 °C, with onset at 635 °C. The use of a monolithic sample shifts the T_c onset to 680 °C and the peak to 800 °C. This effect is explained by the higher heat transfer resistance of bigger particles than the smaller ones [36], but mainly because crystallization of this glass preferentially occurs on the sample surface; the larger surface area of the powder is responsible for crystallization at a lower temperature.

The DSC measurements were essential to define the heat treatments necessary to produce a uniformly crystallized layer on the sample surfaces. The minimum temperature selected was 565 °C and the maximum was 590 °C, the highest temperature for which it was possible to section the sample to measure the crystallized layer thickness and still prevent irreversible self-cracking. Due to the high residual stress related to a thick crystallized layer if treated above 590 °C, the partially crystallized samples shatter during the grinding procedure.

The evolution of texture formed at different temperatures and times is shown in Fig. 3b and c. It was not possible to identify the phases at 565 °C/3 h, because the crystalline fraction is lower than the detection limits. The only phase clearly identified was β-spodumene ($LiAlSi_2O_6$ - ICSD 024897), at 578 °C/4.5 h, which increases intensity as the temperature and time increases. Furthermore, the relative intensities of the peaks change without a trend, indicating that the crystals are mostly aleatory oriented. Fig. 3c compares the XRD patterns of 590 °C/6 h treatment surface of the bulk sample, grounded sample and ICSD pattern. It shows that the spectrum of the ground sample is very similar to the ICSD pattern, indicating that crystals are randomly oriented after grinding. The 100 peak is increased compared to the pattern. The crystal orientation can significantly influence the residual stresses. Nonetheless, for the thermal treatments used in this work, the presence of the other XRD peaks indicates that only a mild texture exists, and, therefore, stress estimate using the average CTE was adopted. The effect of different crystal orientations remains as a perspective for a future work.

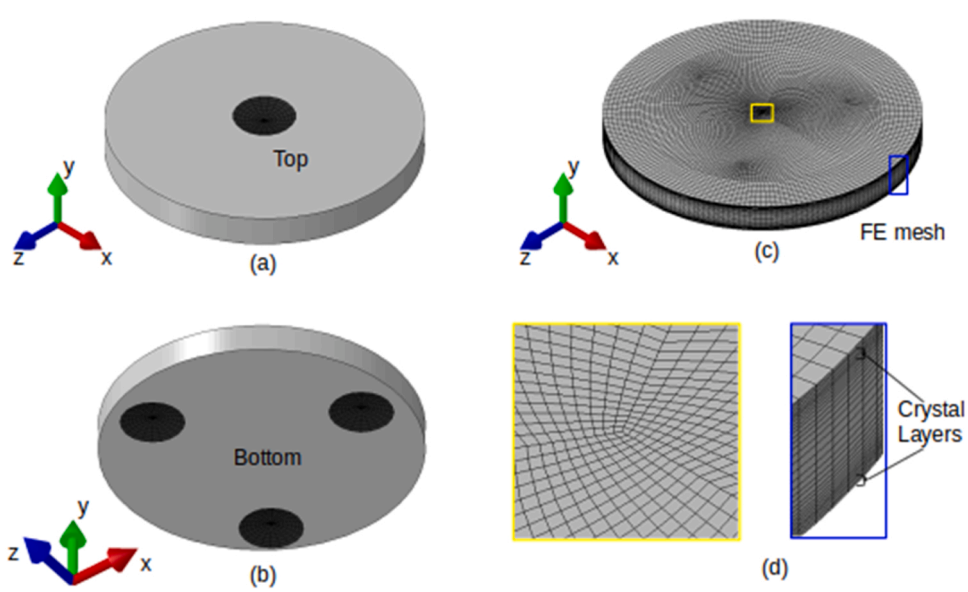

Fig. 2. 3D model for the FE simulation of the B3B test. The analytical rigid surfaces that were used to simulate the balls that apply the y-direction load can be seen one at the top (a) and three at the bottom (b) view. The mesh is shown in (c) and a zoomed view of the disk center and the discretization of the top and bottom crystal layers are shown in (d).

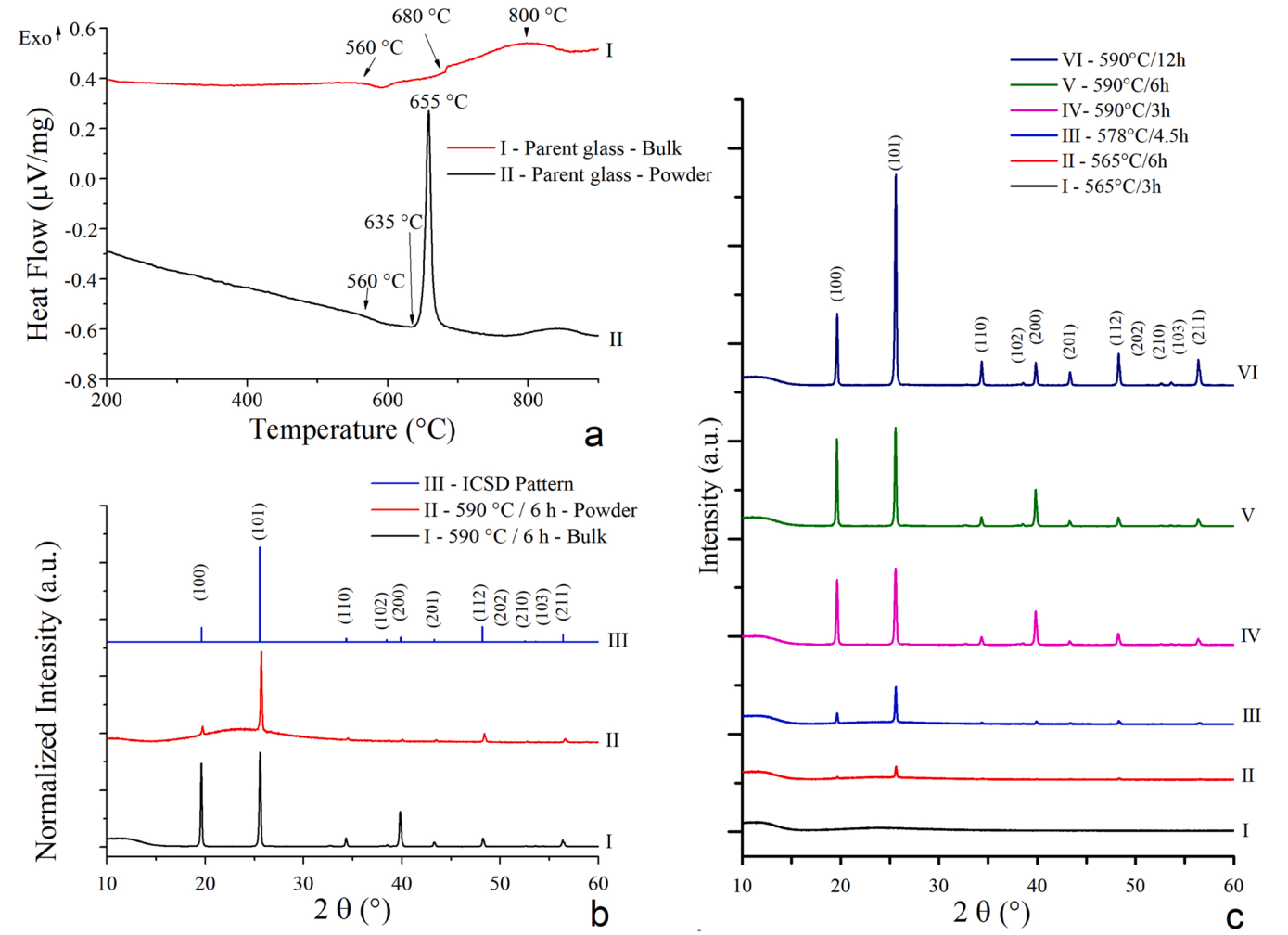

Fig. 3. (a) DSC plot of the LAS parent glass in powder and bulk forms, showing the T_g and the T_c. XRD patterns of LAS GC; (b) patterns for 590 °C/6 h treatment on a monolithic, a ground sample and the ICSD pattern; and (c) surface treated at different temperatures and times: I) 565 °C/3 h; II) 565 °C/6 h; III) 578 °C/4.5 h; IV) 590 °C/3 h; V) 590 °C/6 h and VI) 590 °C/12 h;.

The surfaces of the glass-ceramics resulting from different thermal treatments are shown in Fig. 4. Fig. 5 and Table 2 show the effect of time and temperature on the average crystal size and crystallinity on the glass surface. For the lowest temperature used, the time increment increases the average crystal size from 9 ± 4–13 ± 10 μm. This behavior is not observed for the treatment at the highest temperature used (590 °C), which, considering the error, leads to similar crystal size, 45 ± 15 and 43 ± 12 μm for 3 and 6 h, respectively. Hence, crystal growth saturates sometime before 3 h at this temperature.

The layer thicknesses and the crystal sizes on the sample surface increase as the temperature increases. However, for any situation, the layer thickness is smaller than the average surface crystal size. This difference is because the reported layer thickness is just an average of several measurements of the layer taken at different points and does not represent the maximum size of any single crystal. Furthermore, it is well-known that the growth velocity depends on the crystalline orientation, which is probably different on the surface and in the bulk. Besides, surface growth is enhanced by faster diffusion rates.

According to Priller et. al [17], β-spodumene transforms from the metastable β-eucryptite after some time at any temperature, and could be detected after treating for 24 h at approximately 600 °C. Furthermore, the threshold time to detect crystallization for a treatment at the T_g (550 °C) of their glass was 10 h.

Although the crystallization percentages reported in [18] are only semi-quantitative, the values are similar to our results. After 3 h at 565 °C, the first crystals appear, and after 6 h, the surface crystallized fraction increased and was almost fully crystallized. However, 3 h are likely not enough to promote complete crystallization, as demonstrated by Fig. 5, which compares our results to Priller's [18].

Considering the percentage of crystallization shown in Table 3, it is obvious that on reaching 100% crystallization after ~3 h at 590 °C, surface crystal growth stops. However, the crystallization front continues towards the interior of the glass specimen, increasing the crystal layer thickness. These results indicate that (for the current number of surface nucleated crystals after grinding with 1200 paper) it is not possible to generate a completely crystallized surface layer with crystals smaller than 12 μm. Hence, to decrease the average grain size, the temperature should be lowered and time should be over 6 h. Alternatively, we could further grind the sample surfaces to create a larger number of surface nucleation sites. A major issue for this finding concerns the cracking tendency of this composition. Other authors [23,24] demonstrated self-cracking due to β-eucryptite crystals in the interior of a 48 SiO_2, 38 Al_2O_3, 10 Li_2O, 4 TiO_2 wt% glass and also for cold-pressed eucryptite ceramics. Due to the large CTE anisotropy, they self-cracked for grain sizes over 4 μm. This finding corroborates the cracking tendency of this sample, once the phase observed (β-spodumene) also has a large CTE anisotropy.

As shown in Fig. 6, for temperatures below 590 °C (Fig. 5d), the crystallized layer is very superficial and only a few crystals grow. For the treatment at 565 °C for 3 h, it was difficult to find any crystals on a

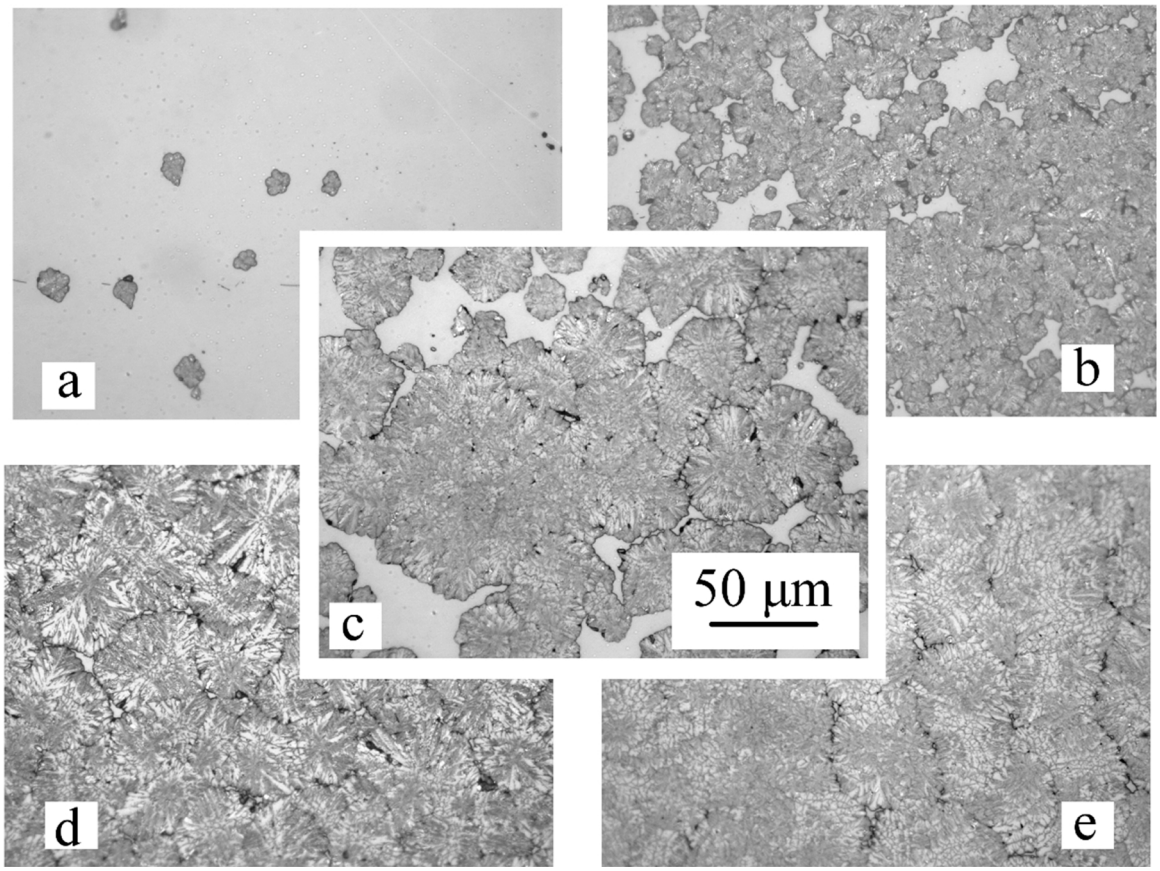

Fig. 4. Optical micrographs of glass-ceramic surfaces after treating the parent glass for: (a) 3.0 h at 565 °C, (b) 6.0 h at 565 °C, (c) 4.5 h at 577.5 °C, (d) 3.0 h at 590 °C and (e) 6.0 h at 590 °C.

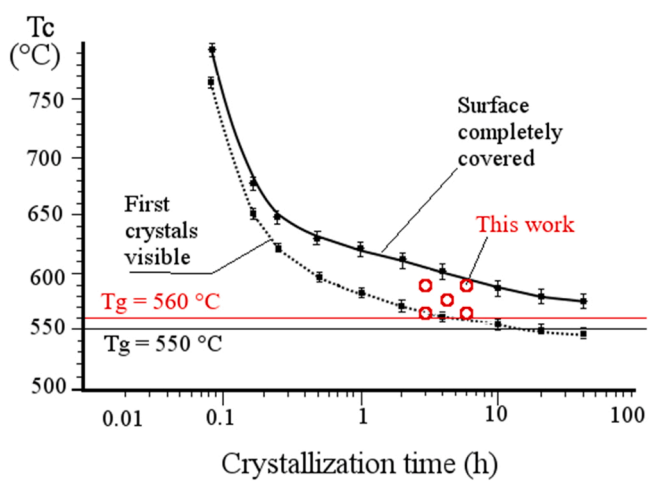

Fig. 5. The dashed lines represent the first crystal visualization with an optical microscope, the solid line shows the fully crystallized surface, both from ref. [17], whereas the red circles show treatments of this work. The Tg of the (similar) present work and the cited work are presented as horizontal lines. Influence of time and temperature on crystallization of the parent glass adapted from Ref. [17]

Table 2
Value of the average crystal size, surface crystallized percentage, and layer thickness for the heat treatments used (± standard deviation).

Treatment condition		Crystal size (μm)	Surface crystallinity (%)	Layer thickness (μm)
a	565 °C / 3 h	9 ± 4	1 ± 1	5 ± 2
b	565 °C / 6 h	13 ± 10	3 ± 2	9 ± 2
c	577.5 °C / 4.5 h	27 ± 14	53 ± 19	14 ± 6
d	590 °C / 3 h	45 ± 15	90 ± 15	24 ± 8
e	590 °C / 6 h	43 ± 12	99 ± 1	56 ± 16

Table 3
Effect of different layer thickness on the indentation nanohardness (H_{IT}), Young's Modulus determined by nanoindentation (E_{IT} and E*) and determined by sound propagation (E).

Property	Parent glass	585 °C 6 h	590 °C 6 h	590 °C 9 h
Layer thickness (μm)	0	40 ± 11	56 ± 7	105 ± 19
Crystal size (μm)	0	40 ± 15	43 ± 12	29 ± 10
H_{IT}	8.0 ± 0.1	8.3 ± 0.2	8.6 ± 0.3	8.5 ± 0.3
E_{IT}	82.6 ± 0.9	78 ± 2	77.1 ± 0.9	79 ± 2
E*	88 ± 1	83 ± 2	82 ± 1	84 ± 2
E	79 ± 2	80 ± 2	80 ± 0	–

transversal section due to the low crystallization percentage, which could also indicate that the induction time for growth in this direction is different from that along the surface plane.

Similar behavior was reported for a surface crystallized μ-cordierite glass-ceramic [37]. In this case, μ-cordierite crystals were texturized, but the growth velocity was similar for any crystalline direction, ranging from 2.9 ± 0.2–3.2 ± 0.2 × 10^{-10} m/s at 860 °C. Nevertheless, the induction times, τ_g, were different for the distinct growth fronts. First, rosettes appeared in the sample interior (τ_g=1.7 ± 0.2 h), followed by elongated hexagons on the surface (2.9 ± 0.2 h), and, finally, a crystallized surface layer (12 ± 1 h).

Additionally, as reported in Fig. 7, the growth velocity from the

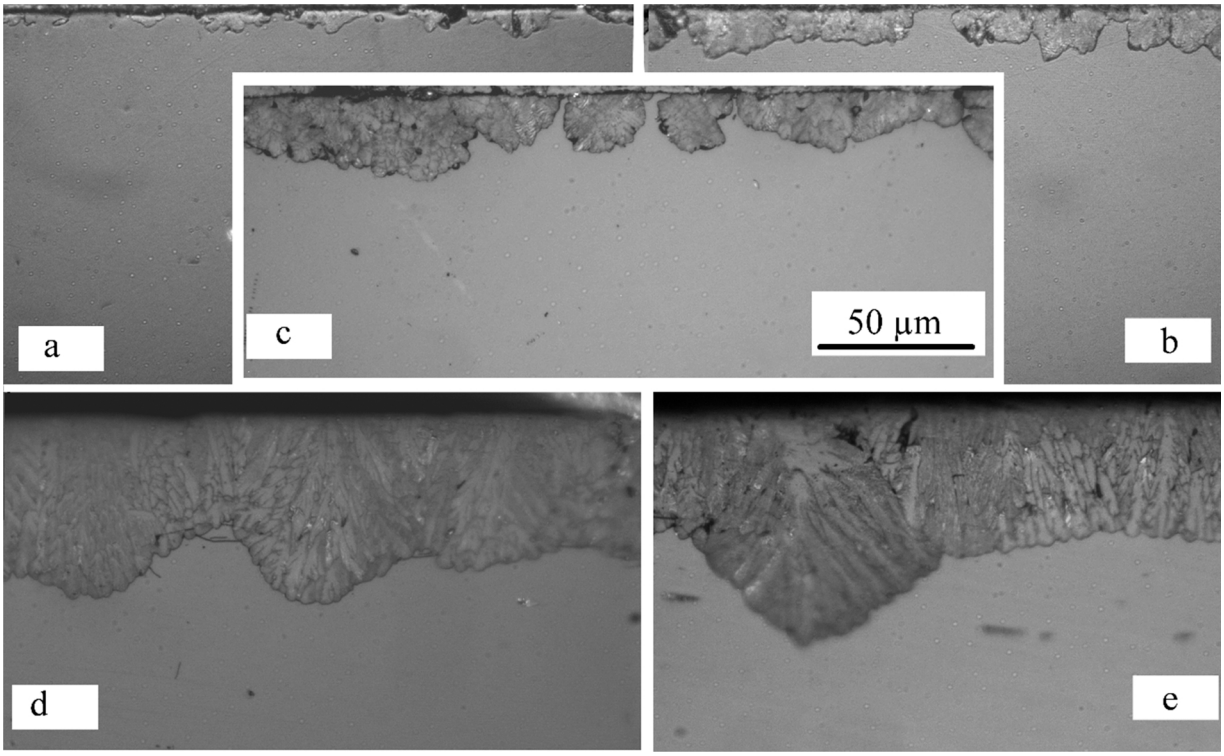

Fig. 6. Effect of time and temperature on the crystalline layer thickness after treating the parent glass for: (a) 3.0 h at 565 °C, (b) 6.0 h at 565 °C, (c) 4.5 h at 577.5 °C, (d) 3.0 h at 590 °C and (e) 6.0 h at 590 °C.

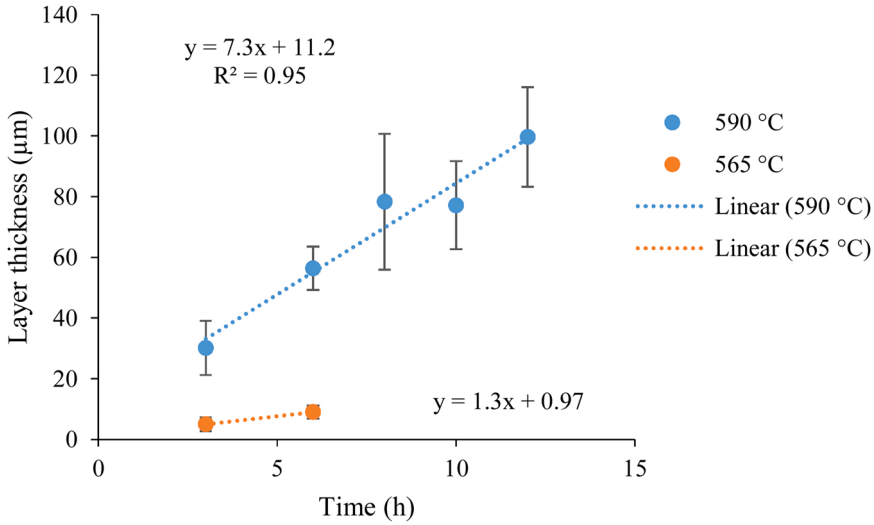

Fig. 7. Crystal growth velocity towards the glass interior.

surface towards the interior could be estimated for the LAS parent glass. The values are similar to those obtained for the Magnesium Aluminum Silicate (MAS) system in [37], resulting in 1.3 µm/h (3.6×10^{-10} m/s) at 565 °C and 7.3 µm/h (20.3×10^{-10} m/s) at 590 °C.

To evaluate the transparency of the current LAS GC, the optical transmittance of a specimen crystallized for 6 h at 590 °C was measured (Fig. 8).

As shown in Fig. 8, a 1.3 mm thick piece of LAS parent glass has over 80% transmittance in the visible range. The surface crystallization process reduces the transmittance to 50–62%. Light scattering is caused by the β-spodumene crystals due to their size on the surface being ~42 µm with a 56 µm thickness. Despite the micrometric grain size, reasonable light transmission occurs due to the similar refractive index of the crystalline phase and glass matrix [38]. Although the refractive index (***n***) of this glass composition has not been reported, the values determined by infrared measurements at 1550 nm are 1.530 and 1.495, for the crystalline (β-spodumene$_{ss}$) and glassy ($73SiO_2$-$12Al_2O_3$-5-Li_2O.2MgO- $2TiO_2$.1 ZrO_2-$2K_2O$-3ZnO (mol%) phases, respectively [39]. The ***n*** values at 20 °C calculated by the Sciglass using the Appen method were 1.518 and 1.514 for the parent and residual glass, respectively. The image is still transmitted integrally when a crystallized 1 mm thick sample is placed on a written paper and observed with the naked eye (see insert in Fig. 8), which suggests this translucence level is reasonable and promising for electronic screens, although it should be further improved for real applications. Nonetheless, it is important to note that using different equipment and techniques of transmittance

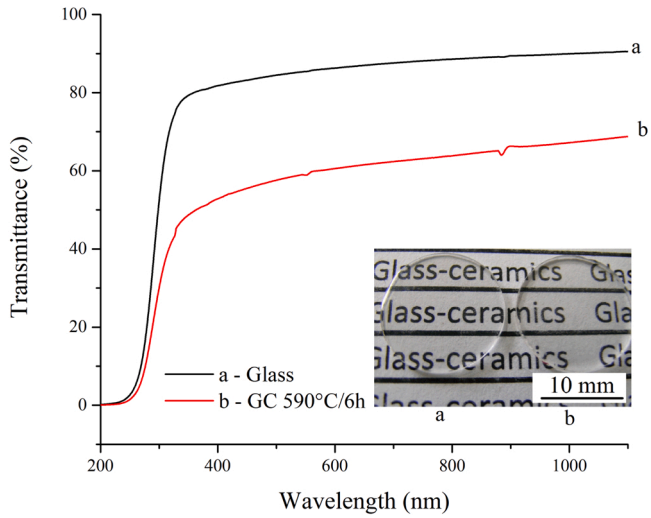

Fig. 8. UV-Vis patterns of 1.3 mm of thick samples. (a) LAS parent glass and (b) GC threated at 590 °C/ 6 h. The insert shows the glass on the left and the GC on the right.

measurement can lead to distinct results.

3.2. Effect of the crystalline layer on the mechanical behaviour

3.2.1. Young's modulus

Table 3 reports the Young's modulus considering the whole crystal/glass "composite" sample and some surface properties determined at the nanoscale (up to 800 nm penetration depth) by indentations on different layer thicknesses.

The Young's modulus determined by the sound propagation technique, which considers propagation throughout the whole sample, is equal for any tested condition, whereas the Young's modulus determined by nanoindentation (surface crystallized layer) is only 4 GPa lower than that of the parent glass.

3.2.2. Hardness

Nanoindentation hardness values of glass-ceramics treated at 590 °C for 6 h are higher than for the parent glass (8.6 GPa *vs.* 8.0 GPa). Nonetheless, there is no difference between crystallized layers from 40 to 105 μm, indicating that at the tested depth there was no effect of the residual stress. This is in agreement with the low variation of Young's Modulus.

The effect of the crystalline layer on the indentation behavior is demonstrated in Fig. 9 and Fig. 10. The considered GC sample was crystallized for 6 h at 590 °C, because at this condition a deeper layer was obtained, making the evaluation easier. This method was chosen due to the micrometric grain size of the current GCs.

The window glass, reported for comparison, shows the usual behavior. The onset load for cracking is 2.94 N and radial cracks can be observed at the 4 corners of indentations [16]. The measured Vickers hardness for this glass at 0.98 N and 1.96 N is 5.7 ± 0.1 GPa.

The LAS parent glass is harder than window glass with a Vickers hardness of 6.3 ± 0.1 GPa at 0.98 N load. The onset for cracking was 9.8 N. This behavior was observed for 4 indentations out of 10 for this load. For the sake of comparison, in an ion-exchange strengthened LAS glass, the hardness at 9.8 N is approximately 5.9 GPa [40] slightly larger than in the bare glass, which is 5.4 GPa, where radial cracks start at 2.94 N and extensive damage occurs at 9.8 N [40]. No indentation size effect (ISE) was observed for the tested glasses.

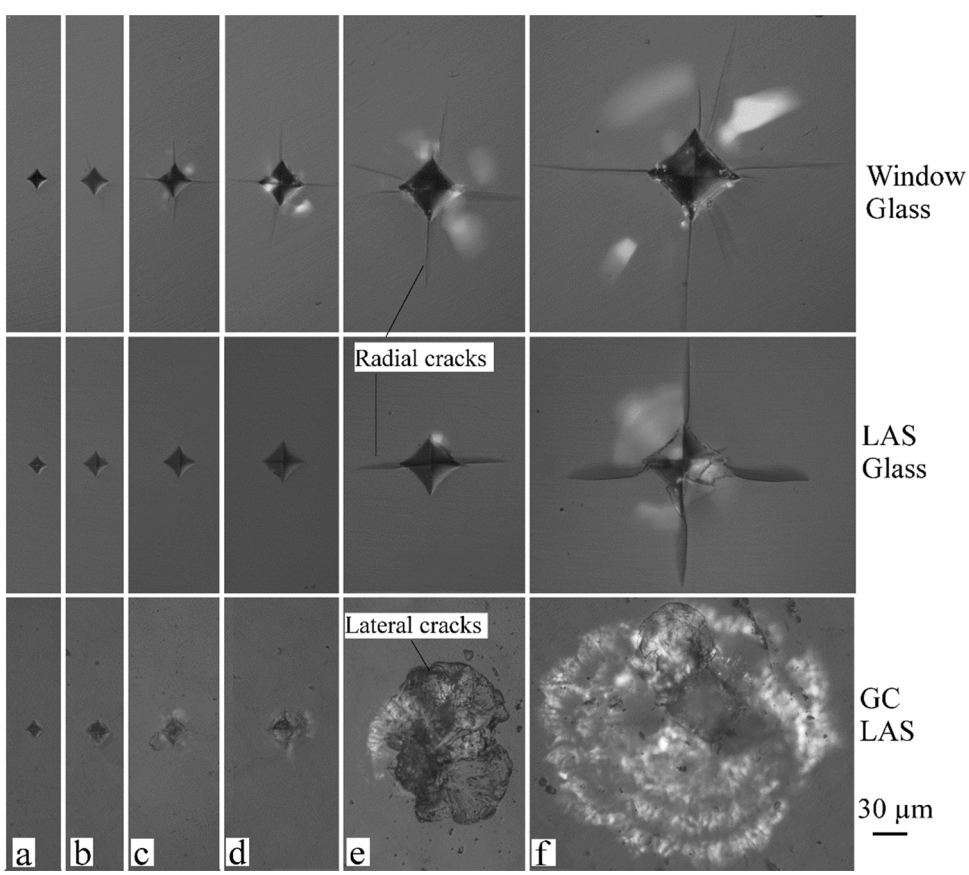

Fig. 9. Vickers indentations at LAS samples (glass and GC crystallized at 590 °C/6 h) and windows glass, with loads of: (a) 0.98 N; (b) 1.96 N; (c) 2.94 N; (d) 4.90 N; (e) 9.8 N; and (f) 19.6 N.

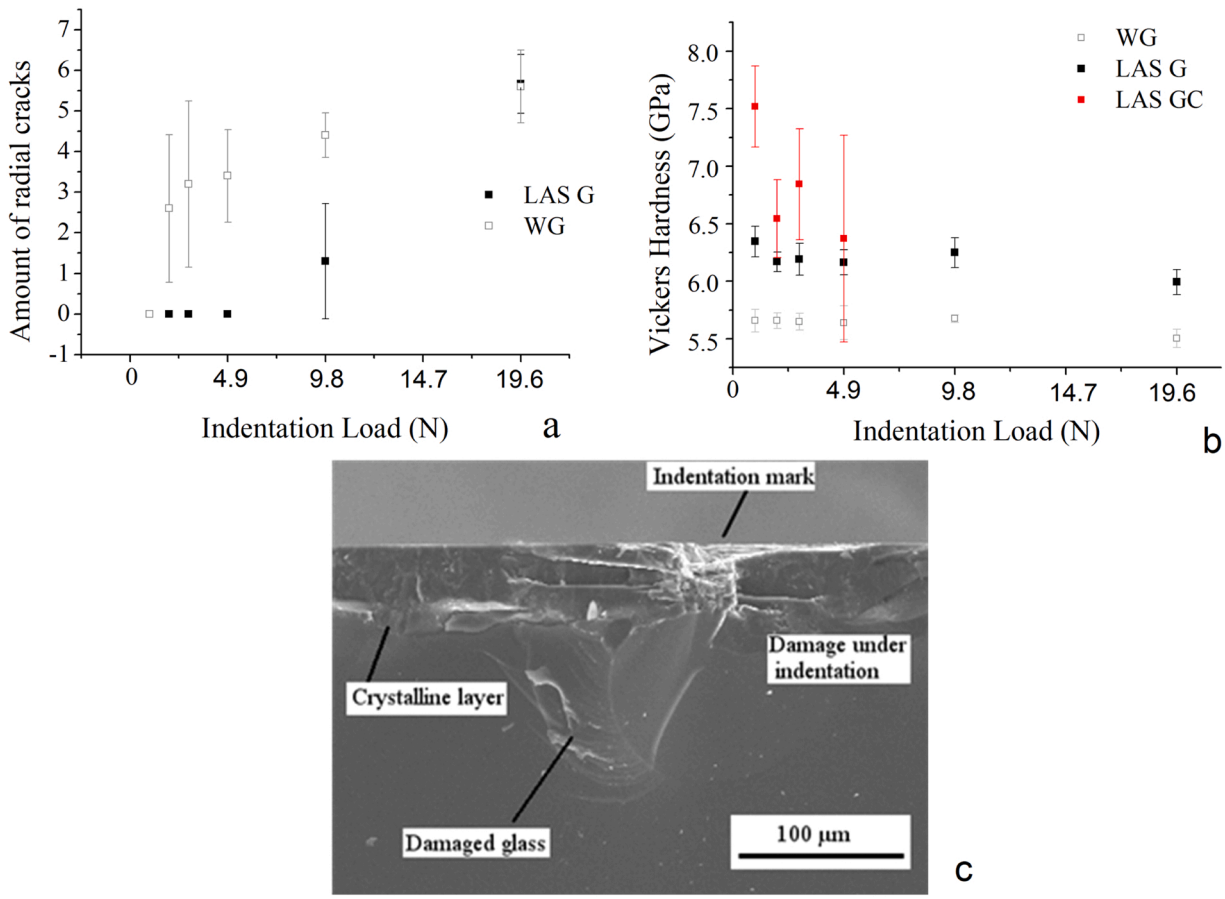

Fig. 10. (a) Vickers hardness at LAS samples (glass and GC treated during 590 °C/6 h) and windows glass (WG) at loads spanning from 0.98 N to 19.6 N; (b) Radial crack probability of tested glasses; (c) Fracture surface of a sample spontaneously broken after 19.6 N Vickers indentation.

The GC shows Vickers hardness imprints smaller than in the precursor glass, although the actual hardness is more difficult to be determined because of the unclear imprint boundaries. No well-developed radial cracks could be observed for any of the used loads, while lateral cracks could be observed on the crystallized layer when applying 9.8 N. For this reason, it was impossible to measure hardness at such load or higher. For the 0.98–4.9 N load range, the GC hardness decreases with the load, thus indicating some ISE. It is interesting to observe that the specimens indented under 1.96 N load spontaneously broke one day after indentation. The fracture surface observed by SEM (Fig. 10c) shows that the indentation-induced damage is deeper than the crystallized layer, thus reaching the region under residual tensile stress.

Moreover, the K_C determined by the indentation method (indentation crack resistance) is 0.9 ± 0.1 MPa.m$^{1/2}$ for the LAS glass and, for comparison, 0.7 MPa.m$^{1/2}$ for window glass. Considering the brittleness index proposed by Sehgal and Ito [16] (H/K_{IC} ratio), the LAS glass is also less brittle than WG. Generally, these effects are related to the chemical structure of glasses, for which more open structures are more resistant to cracking but less resistant to deformation.

3.2.3. Scratch resistance

The scratch resistance results are shown in Fig. 11.

The behavior is similar between the parent glass and the glass ceramic, this being correlated with the equivalent hardness of the two materials. Notwithstanding, the scratch behavior is modified by compressive stresses of GC, whereas cracking is delayed. The cracking behavior can be explained based on critical loads regimes described by Houérou et al. [41]; the micro-ductile regime goes up to 5.8 N and 11.5 N for glass and GC, respectively. At that load, radial cracking and chipping start, characterizing the micro-cracking regime, which ends at

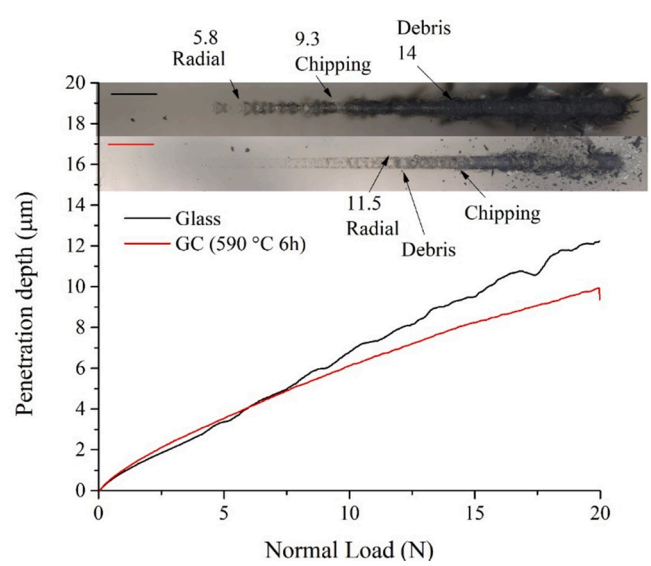

Fig. 11. Scratch resistance of the LAS glass and GC. The optical micrograph shows that the GC has more debris and chipping cracking, whereas the glass shows more radial cracks. The penetration depth in the GC is slightly smaller than in its parent glass.

14 N for glass. The GC has a few radial cracks and several lateral cracks and chipping, which are concomitant with the formation of debris. Hence, the micro-abrasive regime, which is featured by debris and some lateral cracks, also starts at ~11.5 N for the GC and at a slightly higher

load of 14 N for the glass. These findings are similar to those of Ref. [42] for a Magnesium Aluminum Silicate (MAS) glass-ceramic, where the critical load for triggering the micro abrasion region was 13–25 N and was not possible to identify lateral cracks.

3.2.4. Fracture strength

To evaluate the effect of the crystallized layer on the flexural strength, residual stresses were calculated by analytical, numerical and experimental (B3B test) methods for GCs with different crystalline thicknesses. It was observed that by increasing the crystalline thickness, the surface compressive stress reduces according to analytical and axisymmetric numerical calculations, differing no more than 3% among the methods. As the crystalline layer increases, the tensile stress in the glass interior increases. At 350 μm, the crystalline and residual glass layer thicknesses are very similar, resulting in similar absolute values of tensile (interior) and compressive (surface) stresses.

The B3B 3D simulation results are given in Fig. 12, together with their experimental counterparts. A good qualitative trend can be seen, with the maximum normalized load observed in both cases for a crystal in thickness of 9% (*i.e.*, 56 μm layer thickness). At this point, a maximum equivalent stress of 679 ± 48 MPa is found, which diminishes as the crystal layer increases, similarly to what was found in [18] for the same composition and similar thermal treatment. Most of the simulation results are close to the experimental values, the only exception is for a crystal in relative thickness of 0.09 (unitless) with a difference of 17% (about three times the experimental deviation). Considering the several hypotheses, including a constant crystal layer, these differences are deemed very low. It is believed that the correlations could be further improved with considerations of the geometry of crystals and thermal expansion anisotropy, which are out of the scope of the present work. The closeness of the simulated and experimental results corroborates the failure criterion in which the stress state in the outer crystal layer needs to reach the glass internal failure stress for the fracture to take place.

Stress fields for different loadings are shown in Fig. 13 to illustrate the chosen failure criterion. For practical purposes, the 3D model to simulate the B3B experiment had only the upper and lower crystal layers. First, the cooling leads to a compression of 360 MPa in the crystal layer and an internal tensile state of 68 MPa (Fig. 13a). It is worth noting that the difference from this result to the axisymmetric is below 1%. After some mechanical loading, at half of the ultimate force, the tensile stress at the interior was already above the strength of the glass, but the external layer compression could still hold it intact (Fig. 13b). For the ultimate load (Fig. 13c), when the stresses at the outer layer reach the glass strength, the stress in the interior is considerably higher than the strength, which corroborates with the shattering fracture seen in experiments.

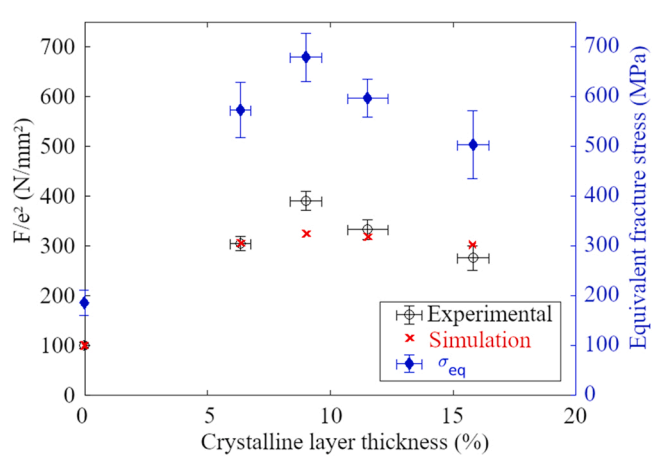

Fig. 12. The B3B maximum force normalized by the square of the thickness (e) is shown at the left y-axis, comparing the 3D FE simulation (red) with the experimental results (black). The equivalent stress (blue), calculated considering a homogeneous media (see Eqs. 1 and 2), is shown in the right y-axis.

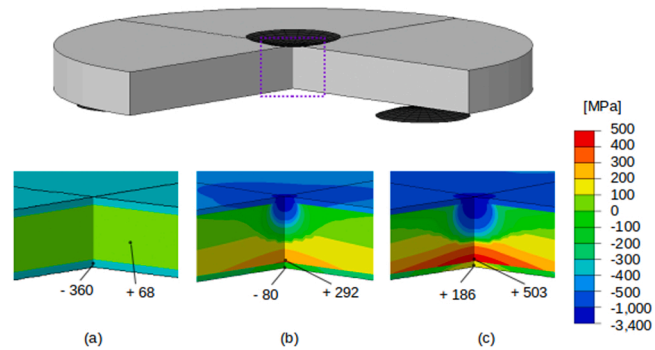

Fig. 13. Maximum absolute value of principal stress for the case with a crystal layer of about 100 μm: (a) after cooling and before the B3B test; (b) at 50% of the ultimate force, and; (c) at the ultimate force. Positive for tension and negative for compression. Note that the glass strength is 186 MPa.

3.3. Spontaneous cracking of the glass-ceramics

As we explained in the last section, the increment of the crystallized layer leads to tensile stresses on the sample interior. Moreover, in this region, the crystallization front results in some residual glass pockets. Once the nominal β-spodumene composition is $1Li_2O$-$1Al_2O_3$-$4SiO_2$ and the parent composition is (in addition to the other components) $1Li_2O$-$1Al_2O_3$-$5.4SiO_2$ (normalized for 1 mol of Li_2O), the composition of the residual glass consists of a network of SiO_2 plus the modifiers K, Ca, Mg and Na without any or poorer in Li and Al_2O_3. These pockets can be observed in the optical micrograph of Fig. 14a,b, which shows a sample cross-section after complete and partial removal of the crystalline layer. In the first, cracks initiate in the stressed region. However, it should be noted that this region was ground for microscopy observation and cracks are probably not present in materials that were not subjected to grinding. Nevertheless, this result confirms this region as a weak point to generate cracks. In the second micrograph, cracks propagate preferentially in the glass phase.

The axisymmetric simulation was performed to check the effects of the corners and the lateral crystal layer on the cooling step. If no rounding is accounted for (Figure 14cI), the tensile stress in the residual glass reaches very high values, above the compression absolute value from the outer layer. When some rounding is used in the interface, *e.g.,* 10 μm or 50 μm (Fig. 14 cII and cIII), keeping the crystal layer thickness constant, the tensile stress is considerably reduced to levels below the compression level. It is worth noting that some samples exploded during cooling when the corners were not ground before the thermal treatment. From these observations, the hypothesis that the residual compression stress from the external layer may hold the fragile fracture of the interior glass until the external compression is overcome seems plausible. Moreover, the stress at the disk center (not shown in Fig. 14) changes very little independently whether the corner is rounded off or not (less than 0.2%), or in the absence of the lateral crystal layer (about 1%).

Although we have shown that grinding the corners before the thermal treatment can diminish the chance for spontaneous shattering, by different causes can lead to spontaneous cracking. It should be pointed out that crystallization leads to a residual glass with different chemical composition, which could be stronger or weaker than the parent glass, although the strength is not expected to change much with chemical composition. Crystallization also generates grain boundaries, which are "defects" and could explain these differences. Finally, the current spherulitic crystals normally have some residual glass in their interior, which can be further stressed. Lastly, the CTE anisotropy within each crystal can also lead to microcracking. Similarly, the microstructural features, such as heterogeneous crystal size depth usually represent a

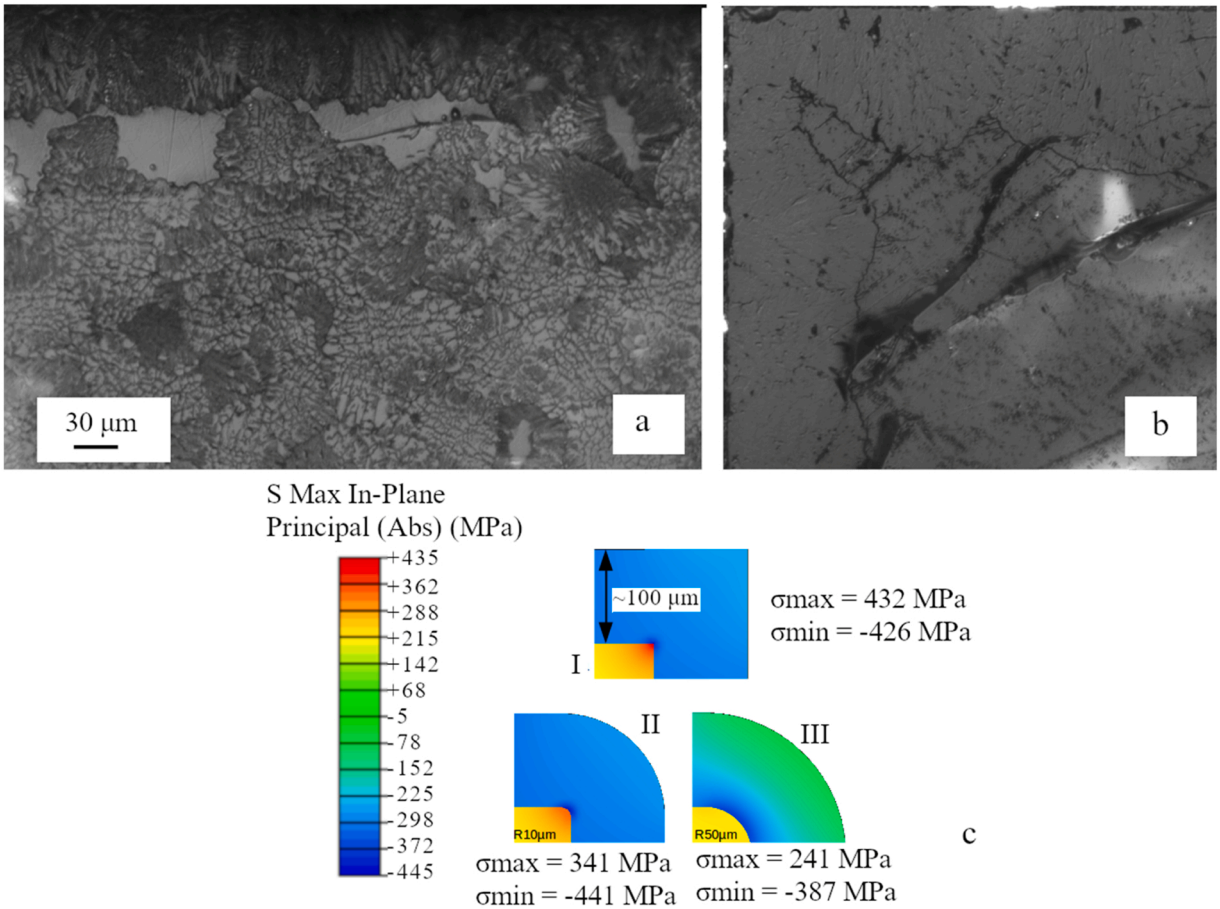

Fig. 14. Optical micrographs of a transversal surface after removing the crystal layer on the observed surface: (a) partially; (b) completely on corner; and (c) Maximum absolute principal stresses for cases with no rounding (I) or rounded at the corner interface with a 10 µm (II) or 50 µm radius (III). The positive (negative) sign indicates that a tensile (compressive) stress is predominant at a given point. The remote stress (*i.e.,* in the middle of the disk) was − 358 MPa in the crystal layer and 71 MPa in the internal glass, with differences below 0.2% between these three cases.

crack source. Hence, there are many possibilities for self-cracking, which should be explored in a future study.

4. Summary and conclusions

In this work, we produced surface crystallized lithia-alumina-silica glass-ceramics with different crystallized layer thicknesses and analysed their role on the generation of residual stress fields and the effect on some mechanical properties.

The magnitude of the residual compressive stress in the crystal layer was estimated by analytical, numerical, and experimental methods, reaching from 360 MPa to 400 MPa. The compressive stresses on the GC surfaces prevented radial crack generation in microhardness and scratch tests. Out of the thermal treatments investigated, the best overall results were obtained by the glass-ceramic treated at 590 °C for 6 h, which achieved a Vickers hardness of 7.5 GPa, only 10 µm penetration in a 20 N scratch test, and a fracture strength of 680 ± 50 MPa in ball-on-three-ball tests. In addition to this very high strength, some of the glass-ceramics are translucent, providing 50–60% transmittance (1.3 mm tick sample) over the visible spectrum.

This study suggests that surface crystallization can be an advantageous technique for developing very high strength, translucent glass-ceramics, which could be useful for a number of applications.

Declaration of Competing Interest

The authors declare that they have no known competing financial interests or personal relationships that could have appeared to influence the work reported in this paper.

Acknowledgments

This study was financed in part by the Coordenação de Aperfeiçoamento de Pessoal de Nível Superior - Brazil (CAPES) - Finance Code 001. We acknowledge the Conselho Nacional de Desenvolvimento Científico e Tecnológico for doctoral funding #142289/2017-5 – Brazil (CNPq), the Coordenação de Aperfeiçoamento de Pessoal de Nível Superior / Programa Institucional de Internacionalização for funding #88887.369172/2019-00 – Brazil (CAPES/PrInt), and the São Paulo Research Foundation (FAPESP) for the CEPID grant #2013/07793-6 for generous funding, for the internship student funding #2019/12417-0, for complementary funding #2020/08077-6 and for the doctoral funding #2018/23081-0.

References

[1] J. Deubener, M. Allix, M.J. Davis, A. Duran, T. Höche, T. Honma, T. Komatsu, S. Krüger, I. Mitra, R. Müller, S. Nakane, M.J. Pascual, J.W.P. Schmelzer, E. D. Zanotto, S. Zhou, Updated definition of glass-ceramics, J. Non Cryst. Solids 501 (2018) 3–10, https://doi.org/10.1016/j.jnoncrysol.2018.01.033.
[2] A.K. Varshneya, Stronger glass products: lessons learned and yet to be learned, Int. j. Appl. Glass Sci. (2018), https://doi.org/10.1111/ijag.12341.
[3] T. Benitez, S.Y. Gómez, A.P.N. de Oliveira, N. Travitzky, D. Hotza, Transparent ceramic and glass-ceramic materials for armor applications, Ceram. Int. 43 (2017) 13031–13046, https://doi.org/10.1016/j.ceramint.2017.07.205.

[4] Y.S. Choi, J.U. Yun, S.E. Park, Flat panel display glass: current status and future, J. Non Cryst. Solids 431 (2016) 2–7, https://doi.org/10.1016/j.jnoncrysol.2015.05.007.
[5] J. Lu, Z. Cao, C. Huang, K. Xiao, A. Street, Y. Dai, Microelectronics reliability failure analysis of projected capacitance touch panel liquid crystal displays – two case studies, Microelectron. Reliab. (2017) 26–29, https://doi.org/10.1016/j.microrel.2017.06.028.
[6] L. Wondraczek, J.C. Mauro, J. Eckert, U. Kühn, J. Horbach, J. Deubener, T. Rouxel, Towards ultrastrong glasses, Adv. Mater. 23 (2011) 4578–4586, https://doi.org/10.1002/adma.201102795.
[7] V.V. Putrolaynen, A.M. Grishin, I.V. Rigoev, Anti-Scratch AlMgB 14 Gorilla ® glass, Coating 43 (2017) 871–874, https://doi.org/10.1134/S1063785017100108.
[8] C.R. Kurkjian, P.K. Gupta, R.K. Brow, The strength of silicate glasses: what do we know, what do we need to know? Int. J. Appl. Glas. Sci. 1 (2010) 27–37.
[9] K. Łączka, K. Cholewa-Kowalska, M.-roda, J. Rysz, M.M. Marzec, M. Łączka, Glass-ceramics of LAS (LiO_2-Al_2O_3-SiO_2) system enhanced by ion-exchange in KNO salt bath, J. Non Cryst. Solids 428 (2015) 90–97.
[10] Corning, 2018. Gorilla Glass - Product Information, (2018).
[11] X. Chen, A.H.C. Chan, J. Yang, Simulating the breakage of glass under hard body impact using the combined finite-discrete element method, Comput. Struct. 177 (2016) 56–68, https://doi.org/10.1016/j.compstruc.2016.08.010.
[12] C. Alter, S. Kolling, J. Schneider, An enhanced non–local failure criterion for laminated glass under low velocity impact, Int. J. Impact Eng. 109 (2017) 342–353.
[13] E. News, 2020. Is "iPhone 12″ unbreakable with "Ceramic Shield"? – Erm News, (2020). 〈https://www.eg24.news/2020/10/is-iphone-12-unbreakable-with-ceramic-shield-erm-news-2.html〉.
[14] Jerryrigeverything, 2020. iPhone 12 Pro Durability Test - Is "Ceramic Shield" Scratchproof?!, (2020). 〈https://www.youtube.com/watch?v=LP6ppSM3xq4〉.
[15] M.E. Broz, R.F. Cook, D.L. Whitney, Microhardness, toughness, and modulus of Mohs scale minerals, Am. Mineral. 91 (2006) 135–142, https://doi.org/10.2138/am.2006.1844.
[16] J. Sehgal, S. Ito, Brittleness of glass, J. Non Cryst. Solids 253 (1999) 126–132.
[17] S. Priller, G.H. Frischat, L.D. Pye, Strengthening of glass through surface crystallization of b-spodumene$_{ss}$, J. Non Cryst. Solids 196 (1996) 144–149.
[18] C. Bocker, C. Funke, C. Rüssel, Strengthening of a zinc silicate glass by surface crystallization, Mater. Lett. 207 (2017) 41–43, https://doi.org/10.1016/j.matlet.2017.07.045.
[19] G.J. Fine, M.E. Greene, 1992. Strong, Surface Crystallized Glass Articles, US 5084328, 1992.
[20] J.P. Pressau, 1969. Method for Producing Surface Compression in Certain Glasses by Promoting Random Surface Crystallization, US 3464807, 1969.
[21] W. Kiefer, W. Sack, D.D. Krause, 1975. Making Surface Crystallized Glass Bodies And Resulting Product, US 3,907,577, 1975.
[22] R.W. Petticrew, C.E. Schott, W.E. Smith, 1970. Art of Producing High-Strength, Surface-Crystallized, Glass Bodies, US 3490984, 1970. https://doi.org/10.1145/178951.178972.
[23] A. Pelletant, H. Reveron, J. Chêvalier, G. Fantozzi, L. Blanchard, F. Guinot, F. Falzon, Grain size dependence of pure β-eucryptite thermal expansion coefficient, Mater. Lett. 66 (2012) 68–71, https://doi.org/10.1016/j.matlet.2011.07.107.
[24] A. Shyam, J. Muth, E. Lara-Curzio, Elastic properties of β-eucryptite in the glassy and microcracked crystalline states, Acta Mater. 60 (2012) 5867–5876, https://doi.org/10.1016/j.actamat.2012.07.028.
[25] T. Waurischk, C. Thieme, C. Rüssel, Crystal growth velocities of a highly anisotropic phase obtained via surface and volume crystallization of barium–strontium–zinc silicate glasses, J. Mater. Sci. 55 (2020) 10364–10374, https://doi.org/10.1007/s10853-020-04773-6.
[26] M. Kracker, L. Vladislavova, C. Thieme, T. Zscheckel, K. Thieme, T. Höche, C. Rüssel, Surface crystallization of low thermal expansion Ba0.5Sr0.5Zn2Si2O7 from an 8 BaO·8 SrO·34 ZnO·50 SiO_2 glass, RSC Adv. 7 (2017) 44834–44842, https://doi.org/10.1039/c7ra08587g.
[27] M. de, O.C. Villas Boas, Desenvolvimento e caracterização de vitrocerâmicos leves e transparentes para proteção balística, São Carlos - SP (2015).
[28] M. Teotia, R.K. Soni, Applications of finite element modelling in failure analysis of laminated glass composites: a review, Eng. Fail. Anal. 94 (2018) 412–437, https://doi.org/10.1016/j.engfailanal.2018.08.016.
[29] T. Pyttel, H. Liebertz, J. Cai, Failure criterion for laminated glass under impact loading and its application in finite element simulation, Int. J. Impact Eng. 38 (2011) 252–263, https://doi.org/10.1016/j.ijimpeng.2010.10.035.
[30] A. Boerger, P. Supancic, R. Danzer, The ball on three balls test for strength testing of brittle discs: stress distribution in the disc, J. Eur. Ceramic Soc. 22 (2002) 1425–1436.
[31] J. Jiusti, D.R. Cassar, E.D. Zanotto, Which glass stability parameters can assess the glass-forming ability of oxide systems? Int. J. Appl. Glass Sci. 11 (2020) 612–621, https://doi.org/10.1111/ijag.15416.
[32] A.M. Rodrigues, L.D. Silva, R. Zhang, V.O. Soares, Structural effects on glass stability and crystallization, CrystEngComm 20 (2018) 2278–2283, https://doi.org/10.1039/c7ce02135f.
[33] J. Jiusti, 2020. Estabilidade e habilidade de formação de vidros óxidos, Universidade Federal de São Carlos, 2020.
[34] W.C. Oliver, G.M. Pharr, An improved technique for determining hardness and elastic-modulus using load and displacement sensing indentation experiments, J. Mater. Res. 7 (1992) 1564–1583, https://doi.org/10.1557/.
[35] G.R. Anstis, Indentation and fracture toughness I, Transformation 46 (1981) 533–538.
[36] V.C.S. Reynoso, K. Yukimitu, T. Nagami, C.L. Carvalho, J.C.S. Moraes, E.B. Arau, 2003. Crystallization kinetics in phosphate sodium-based glass studied by DSC technique, 64 (2003) 27–30.
[37] N. Diaz-Mora, E.D. Zanotto, R. Hergt, R. Müller, Surface crystallization and texture in cordierite glasses, J. Non Cryst. Solids 273 (2000) 81–93, https://doi.org/10.1016/S0022-3093(00)00147-2.
[38] G.H. Beall, D.A. Duke, Transparent Glass-Ceram. 4 (1969) 340–352.
[39] A. Sakamoto, S. Yamamoto, Infrared optical properties of β-spodumene solid solution glass-ceramic for fiber-optic devices, Jpn. J. Appl. Phys., Part 1 Regul. Pap. Short. Notes Rev. Pap. 45 (2006) 6969–6973, https://doi.org/10.1143/JJAP.45.6969.
[40] P. Jannotti, G. Subhash, P. Ifju, P.K. Kreski, A.K. Varshneya, Influence of ultra-high residual compressive stress on the static and dynamic indentation response of a chemically strengthened glass 32 (2012) 1551–1559, https://doi.org/10.1016/j.jeurceramsoc.2012.01.002.
[41] V. Le Houérou, J.C. Sangleboeuf, S. Dériano, T. Rouxel, G. Duisit, Surface damage of soda-lime-silica glasses: Indentation scratch behavior, J. Non Cryst. Solids 316 (2003) 54–63, https://doi.org/10.1016/S0022-3093(02)01937-3.
[42] I.C.J. Dechandt, P. Soares, M.J. Pascual, F.C. Serbena, Sinterability and mechanical properties of glass-ceramics in the system SiO_2-Al_2O_3-MgO/ZnO, J. Eur. Ceram. Soc. 40 (2020) 6002–6013, https://doi.org/10.1016/j.jeurceramsoc.2020.07.032.